

# NEUTRINO AND ANTI-NEUTRINO ENERGY LOSS RATES DUE TO IRON ISOTOPES SUITABLE FOR CORE-COLLAPSE SIMULATIONS

JAMEEL-UN NABI<sup>1,2</sup>

<sup>1</sup>Faculty of Engineering Sciences, Ghulam Ishaq Khan Institute, of Engineering Sciences and Technology, Topi 23640, Swabi, Khyber Pakhtunkhwa, Pakistan  
Email:jameel@giki.edu.pk

<sup>2</sup>Current Address: The Abdus Salam ICTP, Strada Costiera 11, 34014, Trieste, Italy

*Compiled August 20, 2014*

Accurate estimate of neutrino energy loss rates are needed for the study of the late stages of the stellar evolution, in particular for cooling of neutron stars and white dwarfs. The energy spectra of neutrinos and antineutrinos arriving at the Earth can also provide useful information on the primary neutrino fluxes as well as neutrino mixing scenario (it is to be noted that these supernova neutrinos are emitted after the supernova explosion which is a much later stage of stellar evolution than that considered in this paper). Recently an improved microscopic calculation of weak-interaction mediated rates for iron isotopes was introduced using the proton-neutron quasiparticle random phase approximation (pn-QRPA) theory. Here I present for the first time the fine-grid calculation of the neutrino and anti-neutrino energy loss rates due to  $^{54,55,56}\text{Fe}$  in stellar matter. In the core of massive stars isotopes of iron,  $^{54,55,56}\text{Fe}$ , are considered to be key players in decreasing the electron-to-baryon ratio ( $Y_e$ ) mainly via electron capture on these nuclide. Core-collapse simulators may find this calculation suitable for interpolation purposes and for necessary incorporation in the stellar evolution codes. The calculated cooling rates are also compared with previous calculations.

*Key words:* neutrino energy loss rates, iron isotopes in stellar matter, pn-QRPA theory, core-collapse supernovae, core-collapse simulations .

*PACS:* 97.10.Cv, 26.50.+x, 23.40.Bw, 21.60Jz

## 1. INTRODUCTION

Neutrino processes and electron capture play pivotal roles in core-collapse supernova explosions. The discovery of neutrino burst from SN1987A by the Kamiokande II group [1] and IMB group [2] energized the research on neutrino astrophysics. According to the stellar evolution theory and the observation data, the burst of neutrino is the first signal from the supernova explosion. The core of a massive star implodes in a time period of 0.5-1 s and around  $10^{53}$  ergs of binding energy of gravity is released, of which only 1% is transferred by neutrinos to eject the envelope of the star. Understanding neutrino interactions in the circumstance of a supernova is pivotal to a better understanding of the explosion mechanism.

During the first tens of seconds of the proto-neutron star's evolution, neutrinos diffuse outward and escape from the star thereby lowering the entropy and lepton abundance of the stellar matter. This scenario does not necessarily hold at extremely high densities and temperatures (this would be the case for stellar collapse where dynamical time scales become shorter than the neutrino transport time scales) where neutrinos can become trapped in the so-called neutrinospheres mainly due to elastic scattering with nuclei. During the late stages of stellar evolution a star mainly loses energy through neutrinos. White dwarfs and supernovae (which are the endpoints for stars of varying masses) have both cooling rates largely dominated by neutrino production. Prior to stellar collapse one requires an accurate determination of neutrino energy loss rates in order to perform a careful study of the final branches of star evolutionary tracks. A change in the cooling rates particularly at the very last stages of massive star evolution could affect the evolutionary time scale and the iron core configuration at the onset of the explosion [3]. The electron capture rates and the accompanying neutrino energy loss rates are also required in determining the equation of state. Reliable and microscopic calculations of neutrino cooling rates and capture rates can contribute effectively in the final outcome of these simulations on world's fastest supercomputers.

The first-ever extensive calculation of stellar weak rates including the capture rates, neutrino energy loss rates and decay rates for a wide density and temperature domain was performed by Fuller, Fowler, and Newman (FFN) [4]. The calculation was done for 226 nuclei in the mass range  $21 \leq A \leq 60$ . The authors stressed on the importance of the Gamow-Teller (GT) giant resonance strength in the capture of the electron and estimated the GT centroids using zeroth-order ( $0\hbar\omega$ ) shell model. The measured data from various (p,n) and (n,p) experiments later revealed the misplacement of the GT centroid adopted in the parameterizations of FFN. Since then theoretical efforts were concentrated on the microscopic calculations of weak-interaction mediated rates of iron-regime nuclide. The proton-neutron quasiparticle random phase approximation (pn-QRPA) theory (e.g. [5]) and the large-scale shell model (LSSM)(e.g. [6]) were used extensively and with relative success for the microscopic calculation of stellar weak rates.

Proton-neutron quasi particle random phase approximation (pn-QRPA) theory and shell model are extensively used for the calculations of capture rates in the stellar environment. Shell model lays more emphasis on interaction of nucleons as compared to correlations whereas pn-QRPA puts more weight on correlations. One big advantage of using pn-QRPA theory is that it gives us the liberty of performing calculations in a luxurious model space (up to  $7\hbar\omega$ ). The pn-QRPA method considers the residual correlations among the nucleons via one particle one hole (1p-1h) excitations in a large model spaces. The prevailing temperature of the stellar matter is of the order of a few hundred kilo-electron volts to a few million-electron volts and  $GT_{\pm}$

transitions occur not only from nuclear ground state, but also from excited states. As experimental information about excited state strength functions seems inaccessible, Aufderheide [7] stressed much earlier the need to probe these strength functions theoretically. Today the pn-QRPA theory calculates the  $GT_{\pm}$  strength distribution of *all* excited states of parent nucleus in a microscopic fashion and this feature of the pn-QRPA model greatly enhances the reliability of the calculated rates in stellar matter. In other words the pn-QRPA model allows a microscopic state-by-state calculation of all stellar weak rates and the Brink hypothesis is not assumed in this model. Brink hypothesis states that GT strength distribution on excited states is *identical* to that from ground state, shifted *only* by the excitation energy of the state. Recent calculations have pointed towards the fact that Brink hypothesis is not a safe approximation to use for calculation of stellar weak-interaction rates [8–12].

During the presupernova evolution of massive stars, the isotopes of iron,  $^{54,55,56}\text{Fe}$ , are advocated to play a key role inside the cores primarily decreasing the electron-to-baryon ratio ( $Y_e$ ) mainly via electron capture processes thereby reducing the pressure support. The neutrinos and antineutrinos produced, as a result of these weak-interaction reactions, are transparent to the stellar matter and assist in cooling the core thereby reducing the entropy. The structure of the presupernova star is altered both by the changes in  $Y_e$  and the entropy of the core material. Calculation of weak-interaction rates of isotopes of iron,  $^{54,55,56}\text{Fe}$ , in stellar matter, were recently calculated using the pn-QRPA model [9]. Later on the detailed analysis of neutrino cooling rates due to these isotopes of iron relevant to the presupernova evolution of massive stars were presented [13]. There the author reported that during the presupernova evolution of massive stars, from oxygen shell burning till around end of convective core silicon burning phases, the pn-QRPA calculated neutrino cooling rates due to  $^{54}\text{Fe}$  were three to four times bigger than the large-scale shell model (LSSM) results [6]. For other phases of presupernova evolution, at times the two rates were in very good comparison, while at other instances the reported neutrino cooling rates were slightly bigger or smaller than the corresponding LSSM rates. The temporal variation of  $Y_e$  depends on how fine the calculated weak rates changes with time. Due to the rather small variation in calculated rates, a fine-grid calculation of stellar neutrino and anti-neutrino energy loss rates due to  $^{54,55,56}\text{Fe}$  was desired by the core-collapse simulators for more accurate outcomes. Due to the extreme conditions prevailing in the cores of massive stars, interpolation of calculated rates within large intervals of temperature-density points posed some uncertainty in the values of cooling rates for collapse simulators. For the first time a fine-grid calculation of neutrino and anti-neutrino energy loss rates in stellar matter due to isotopes of iron is being presented in this paper. The calculation is done using the pn-QRPA model and is presented on a detailed temperature and density grid pertinent to presupernova and supernova environment and should prove more suitable for running on simulation

codes. It is to be noted that throughout this paper (anti)neutrino energy loss rates and (anti)neutrino cooling rates are meant as the same physical phenomena and the two terms are used interchangeably.

Section 2 briefly discusses the formalism of the pn-QRPA model and presents some of the calculated results. Comparison with earlier calculations is also included in this section. I summarize the main conclusions in Section 3. The fine-grid calculation of neutrino and anti-neutrino energy loss rates due to  $^{54,55,56}\text{Fe}$  is presented in a tabular form towards the end of this manuscript.

## 2. CALCULATION AND RESULTS

The neutrino and anti-neutrino energy loss rates of a transition from the  $i$ th state of the parent to the  $j$ th state of the daughter nucleus is given by

$$\lambda_{ij}^{\nu(\bar{\nu})} = \left[ \frac{\ln 2}{D} \right] [f_{ij}(T, \rho, E_f)] \left[ B(F)_{ij} + \left( g_A/g_V \right)^2 B(GT)_{ij} \right]. \quad (1)$$

The value of  $D$  was taken to be 6295s [14].  $B'_{ij}$ s are the sum of reduced transition probabilities of the Fermi  $B(F)$  and GT transitions  $B(GT)$ . Details of the calculations of phase space integrals and reduced transition probabilities in the pn-QRPA model can be found in Refs. [13, 15].

The total (anti)neutrino energy loss rate per unit time per nucleus was then calculated using

$$\lambda^{\nu(\bar{\nu})} = \sum_{ij} P_i \lambda_{ij}^{\nu(\bar{\nu})}. \quad (2)$$

The summation over all initial and final states was carried out until satisfactory convergence in the rate calculations was achieved. Here  $P_i$  is the probability of occupation of parent excited states and follows the normal Boltzmann distribution. The pn-QRPA theory allows a microscopic state-by-state calculation of both sums present in Eq. (2). As discussed earlier this feature of the pn-QRPA model greatly increases the reliability of the calculated rates in stellar matter where there exists a finite probability of occupation of excited states.

The deformation parameter was recently being argued as an important parameter for QRPA calculations at par with the pairing parameter by Stetcu and Johnson [16]. As such rather than using deformations from some theoretical mass model (as used in earlier calculations of pn-QRPA rates e.g. [5, 17]) the experimentally adopted value of the deformation parameters for  $^{54,56}\text{Fe}$ , extracted by relating the measured energy of the first  $2^+$  excited state with the quadrupole deformation, was taken from Raman et al. [18]. For the case of  $^{55}\text{Fe}$  (where such measurement lacks)

the deformation of the nucleus was calculated as

$$\delta = \frac{125(Q_2)}{1.44(Z)(A)^{2/3}}, \quad (3)$$

where  $Z$  and  $A$  are the atomic and mass numbers, respectively, and  $Q_2$  is the electric quadrupole moment taken from Ref. [19].  $Q$ -values were taken from the recent mass compilation of Audi et al. [20].

The incorporation of measured deformations for  $^{54,56}\text{Fe}$  and a smart choice of strength parameters led to an improvement of the calculated  $\text{GT}_{\pm}$  distributions compared to the measured ones [9]. It was shown in Table 1 of Ref. [9] that the present pn-QRPA calculated  $\text{GT}_{\pm}$  centroids and total  $S_{\beta\pm}$  strengths were in good agreement with available data for the even-even isotopes of iron. The table also showed the marked improvement in the reported pn-QRPA calculation over the previous one [5].

In order to further increase the reliability of the calculated capture rates experimental data were incorporated in the calculation wherever possible. In addition to the incorporation of the experimentally adopted value of the deformation parameter, the calculated excitation energies (along with their  $\log ft$  values) were replaced with an experimental one when they were within 0.5 MeV of each other. Missing measured states were inserted and inverse and mirror transitions were also taken into account. No theoretical levels were replaced with the experimental ones beyond the excitation energy for which experimental compilations had no definite spin and/or parity. A state-by-state calculation of  $\text{GT}_{\pm}$  strength was performed for a total of 246 parent excited states in  $^{54}\text{Fe}$ , 297 states for  $^{55}\text{Fe}$  and 266 states for  $^{56}\text{Fe}$ . For each parent excited state, transitions were calculated to 150 daughter excited states. The band widths of energy states were chosen according to the density of states to cover an excitation energy of (15-20) MeV in parent and daughter nuclei. The summation in Eq. (2) was done to ensure satisfactory convergence. The use of a separable interaction assisted in the incorporation of a luxurious model space of up to 7 major oscillator shells which in turn made possible to consider these many excited states both in parent and daughter nucleus.

The calculation of neutrino and anti-neutrino energy loss rates due to  $^{54,55,56}\text{Fe}$  was presented earlier in Ref. [13]. In this paper I would like to present a graphical comparison of these energy loss rates with previous calculations for stellar densities  $\rho Y_e [\text{gcm}^{-3}] = 10^6, 10^7, 10^8$ . The temperature ranges from  $T_9[K] = 1$  to  $T_9[K] = 30$ . This density-temperature domain is particularly important for the presupernova evolution of massive stars (see Ref. [13] for details). The pn-QRPA calculation is compared with the results of large scale shell model (LSSM) [6] and the pioneering calculation of FFN [4].

The pn-QRPA calculated neutrino and anti-neutrino energy loss rates due to  $^{54}\text{Fe}$  is compared against LSSM and FFN calculations in Fig. 1. The upper panel dis-

plays the ratio of calculated rates to the LSSM rates,  $R_{QRPA/LSSM}$ , while the lower panel shows a similar comparison with the FFN calculation,  $R_{QRPA/FFN}$ . Both neutrino and anti-neutrino energy loss rate comparisons are presented in each panel. It can be seen that at low temperatures and densities the calculated neutrino energy loss rates is around five times bigger than those calculated by LSSM. During the oxygen shell burning and silicon core burning phases of massive stars the pn-QRPA energy loss rates are around 3–4 times bigger than LSSM rates. At high temperatures and densities the two calculations are in very good agreement. It is pertinent to mention again that the neutrino energy loss rates contain contributions due to electron capture and positron decay on iron isotopes. Since the electron capture rates are orders of magnitude bigger than the corresponding positron decay rates [9] the neutrino energy loss rate comparison is dictated by the corresponding comparison between electron capture rates. The calculated neutrino energy loss rates due to  $^{54}\text{Fe}$  are up to an order of magnitude smaller as compared to FFN rates at  $\rho Y_e [\text{gcm}^{-3}] = 10^6, 10^7$  and low temperatures (lower panel of Fig. 1). The comparison improves at higher temperatures (where the FFN rates are roughly a factor three bigger). It is to be noted that FFN neglected the quenching of the total GT strength in their rate calculation. The calculated antineutrino energy loss rates contain contributions due to positron capture and  $\beta$ -decay on iron isotopes. Both these contributions are relatively very small as compared to the corresponding electron capture rates. Correspondingly the anti-neutrino energy loss rates are very small in magnitude. These small numbers are fragile functions of the available phase space and can change appreciably by a mere change of 0.5 MeV in phase space calculations and are more reflective of the uncertainties in calculation of the energy eigenvalues (for both parent and daughter states). At  $T_9[K] = 1$  and  $\rho Y_e [\text{gcm}^{-3}] = 10^6$ , the pn-QRPA anti-neutrino energy loss rates are up to four orders of magnitude smaller than the corresponding LSSM rates (upper panel). At high temperatures the two calculations are in reasonable agreement with the pn-QRPA rates bigger by a factor of six. It can be seen that the anti-neutrino energy loss rates are more dependent on the stellar temperatures. The comparison with FFN calculations follows a similar trend (lower panel). However the FFN rates are bigger at all temperature-density domain.

Fig. 2 shows how the calculated energy loss rates compare with previous calculations due to  $^{55}\text{Fe}$ . The upper panel of Fig. 2 shows that LSSM and pn-QRPA calculations agree very well for all important temperature-density domain. The FFN rates are bigger by an order of magnitude at low temperatures and stellar densities in the range  $\rho Y_e [\text{gcm}^{-3}] = 10^6, 10^7$  (lower panel). The probability of occupation of high-lying excited states increases with stellar temperature and FFN did not take into effect the process of particle emission from excited states and accordingly their parent excitation energies extended well beyond the particle decay channel. The anti-neutrino energy loss rates due to  $^{55}\text{Fe}$  are around four orders of magnitude smaller



than LSSM rates at  $T_9[K] = 1$  and  $\rho Y_e[gcm^{-3}] = 10^8$ . At  $T_9[K] = 30$  the pn-QRPA rates are around an order of magnitude bigger (upper panel). The FFN anti-neutrino energy loss rates are up to four orders of magnitude bigger than pn-QRPA rates at low temperatures. The comparison is reasonably well at high temperatures (lower panel).

Comparison of the pn-QRPA calculated neutrino energy loss rates due to  $^{56}\text{Fe}$  with LSSM is again reasonably well (Fig. 3) for the astrophysically important density-temperature domain. The electron capture rates on  $^{56}\text{Fe}$  are very important for the pre-supernova phase of massive stars. FFN rates (lower panel) are again bigger for reasons already mentioned. Regarding the comparison of anti-neutrino energy loss rates the upper panel shows that at low stellar temperatures the LSSM rates are bigger by 1–2 orders of magnitude. The comparison is fairly well at  $T_9[K] = 10$  while at still higher temperatures the pn-QRPA rates are bigger by a factor of 7 for all density range shown in Fig. 3. FFN anti-neutrino energy loss rates are around 4 orders of magnitude bigger at low temperatures. The comparison improves as the stellar temperature increases. For a detailed discussion on the possible reasons for these differences, the reader is referred to Ref. [13].

The fine-grid calculation of pn-QRPA calculated energy loss rates due to  $^{54,55,56}\text{Fe}$  is presented in Table 1. The calculated rates are tabulated in logarithmic (to base 10) scale. The first column gives stellar densities,  $\log(\rho Y_e)$ , in units of  $gcm^{-3}$ , where  $\rho$  is the baryon density and  $Y_e$  is the ratio of the electron number to the baryon number. Stellar temperatures ( $T_9$ ) are given in  $10^9$  K. Stated also are the values of the Fermi energy of electrons in units of MeV.  $\lambda^\nu(\lambda^{\bar{\nu}})$  are the neutrino(anti-neutrino) energy loss rates in units of  $MeV.s^{-1}$ . It is to be noted that Table 1 only shows the calculated rates at a selected density of  $\rho Y_e[gcm^{-3}] = 10^{6.5}$  and  $10^7$ . The complete table is not presented here to save space. Interested readers may find a complete set of table covering stellar density in the range  $\rho Y_e[gcm^{-3}] = 10 - 10^{11}$  as an addendum to the on-line version of this paper. Core-collapse simulators may find Table 1 useful for interpolation purposes and check the consequences of incorporating the reported energy cooling rates due to isotopes of iron in their simulation codes. The ASCII file of Table 1 is also available and can be received from the author upon request.

### 3. SUMMARY

In order to understand the supernova explosion mechanism international collaborations of astronomers and physicists are being sought. Weak interaction mediated rates are key nuclear physics input to simulation codes and a reliable and microscopic calculation of these rates (both from ground-state *and* excited states) is desirable. The pn-QRPA model has a good track record of calculation of weak

interaction rates both in terrestrial and stellar domains. The model has access to a huge model space making it possible to calculate weak rates for arbitrarily heavy system of nucleons. Further the model gets rid of the Brink hypothesis and calculates a *state-by-state* calculation of stellar capture rates which greatly increases the reliability of calculated rates. Incorporation of experimental deformation lead to a much improved version of this calculation. The model was used recently to calculate weak-interaction mediated rates on iron isotopes,  $^{54,55,56}\text{Fe}$  [9].

The main idea of reporting this work is to present a fine-grid calculation of neutrino and anti-neutrino energy loss rates due to  $^{54,55,56}\text{Fe}$  in stellar matter. Table 1 shows the result. As mentioned earlier the complete table can be found in the addendum of the on-line version of this paper. This table can be of great utility for core-collapse simulators and is more convenient for interpolation purposes. The calculation was also compared against LSSM and FFN calculations. The pn-QRPA neutrino energy loss rates due to  $^{54}\text{Fe}$  is around five times bigger than LSSM rates and favor cooler stellar cores. The two calculations are in good agreement for  $^{55,56}\text{Fe}$ . FFN rates on the average are around an order of magnitude bigger.

*Acknowledgements.* The author would like to acknowledge the local hospitality provided by the Abdus Salam ICTP, Trieste, where part of this project was completed. The author wishes to acknowledge the support of research grant provided by the Higher Education Commission, Pakistan through the HEC Project No. 20-1283.

## REFERENCES

1. K. Hirata et al., Phys. Rev. Lett. **58**, 1490 (1987).
2. R. M. Bionta et al., Phys. Rev. Lett. **58**, 1494 (1987).
3. S. Esposito, G. Mangano, G. Miele, I. Picardi and O. Pisanti, Nucl. Phys. B **658**, 217 (2003).
4. G. M. Fuller, W. A. Fowler, M. J. Newman, ApJS **42**, 447 (1980); **48**, 279 (1982); ApJ **252**, 715 (1982).
5. J.-U. Nabi, H. V. Klapdor-Kliengrothaus, Atomic Data and Nuclear Data Tables **88**, 237 (2004).
6. K. Langanke and G. Martínez-Pinedo, Nucl. Phys. A **673**, 481 (2000).
7. M. B. Aufderheide, Nucl. Phys. A **526**, 161 (1991).
8. J.-U. Nabi and M. Sajjad, Phys. Rev. C **77** 055802 (2008).
9. J.-U. Nabi, Eur. Phys. J. A **40**, 223 (2009).
10. J.-U. Nabi, Phys. Scr. **81**, 025901 (2010).
11. J.-U. Nabi, Int. J. Mod. Phys. E **19**, 1 (2010).
12. J.-U. Nabi, Astrophys. Sp. Sc. **331**, 537 (2011).
13. J.-U. Nabi, Adv. Sp. Res. **48**, 985 (2011).
14. G. P. Yost et al. (Particle Data Group), Phys. Lett. B **204**, 1 (1988).
15. J.-U. Nabi, Adv. Sp. Res. **46**, 1191 (2010).
16. I. Stetcu and C. W. Johnson, Phys. Rev. C **69**, 024311 (2004).
17. J.-U. Nabi, H. V. Klapdor-Kliengrothaus, Atomic Data and Nuclear Data Tables **71**, 149 (1999).
18. S. Raman, C. H. Malarkey, W. T. Milner, C. W. Nestor, Jr., and P. H. Stelson, Atomic Data and



Nuclear Data Tables **36 1** (1987).

19. P. Möller and J. R. Nix, Atomic Data and Nuclear Data Tables **26**, 165 (1981).
20. G. Audi, A. H. Wapstra, and C. Thibault, Nucl. Phys. A **729**, 337 (2003).

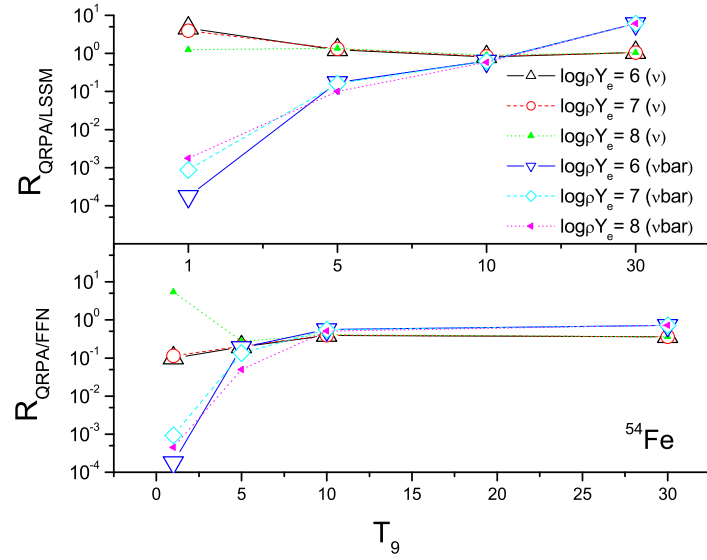
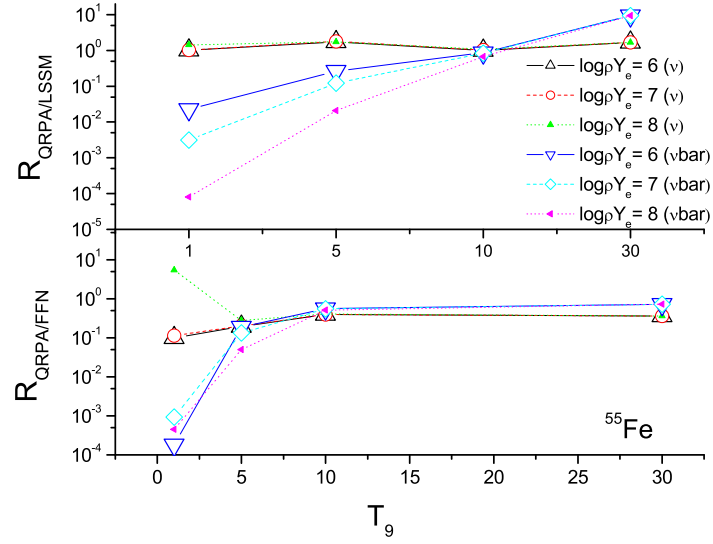
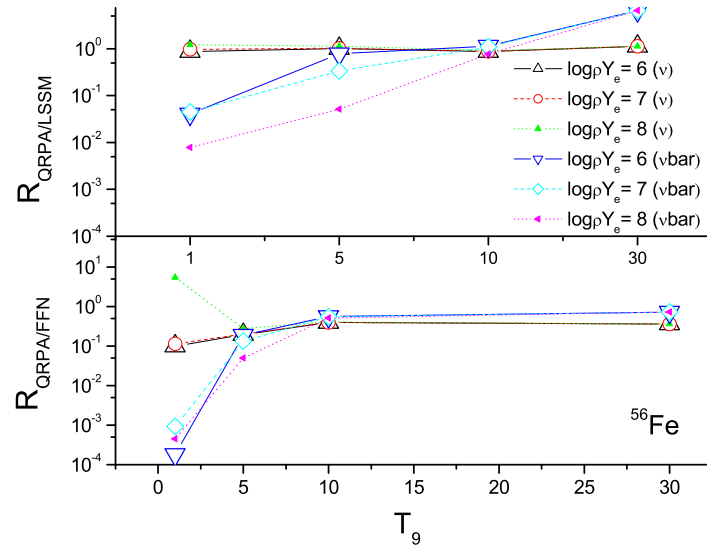


Fig. 1 – (Color online) Ratios of reported neutrino ( $\nu$ ) and anti-neutrino ( $\bar{\nu}$ ) cooling rates due to  $^{54}\text{Fe}$  to those calculated using LSSM [6] (upper panel) and FFN [4] (lower panel) as function of stellar temperatures and densities.  $T_9$  gives the stellar temperature in units of  $10^9$  K. In the legend,  $\log \rho Y_e$  gives the log to base 10 of stellar density in units of  $\text{gcm}^{-3}$ ,  $\nu$  and  $\bar{\nu}$  stand for neutrino and anti-neutrino cooling rate ratios, respectively.

Fig. 2 – (Color online) Same as Fig. 1 but for cooling ratios due to  $^{55}\text{Fe}$ .Fig. 3 – (Color online) Same as Fig. 1 but for cooling ratios due to  $^{56}\text{Fe}$ .

**Table 1:** Calculated neutrino and anti-neutrino energy loss rates due to  $^{54,55,56}\text{Fe}$  on a fine-grid temperature scale. The calculated rates are tabulated in logarithmic (to base 10) scale. The rates are tabulated for a selected density of  $\log \rho Y_e = 6.5$  and 7. For units see text. For complete table see the addendum in the on-line version of this paper.

$\log \rho Y_e$	$T_9$	$E_f$	$^{54}\text{Fe}$		$^{55}\text{Fe}$		$^{56}\text{Fe}$	
			$\lambda_\nu$	$\lambda_{\bar{\nu}}$	$\lambda_\nu$	$\lambda_{\bar{\nu}}$	$\lambda_\nu$	$\lambda_{\bar{\nu}}$
6.5	0.50	0.905	-18.321	-96.473	-5.976	-48.612	-39.992	-59.560
6.5	1.00	0.880	-11.149	-51.087	-5.851	-27.623	-21.887	-32.715
6.5	1.50	0.837	-8.661	-34.623	-5.653	-19.939	-15.468	-22.696
6.5	2.00	0.777	-7.303	-26.161	-5.320	-15.620	-12.113	-17.365
6.5	2.50	0.701	-6.373	-20.942	-4.907	-12.889	-10.025	-14.035
6.5	3.00	0.612	-5.656	-17.358	-4.511	-10.983	-8.584	-11.727
6.5	3.50	0.517	-5.067	-14.726	-4.155	-9.554	-7.513	-10.013
6.5	4.00	0.424	-4.561	-12.710	-3.830	-8.429	-6.667	-8.684
6.5	4.50	0.343	-4.110	-11.120	-3.524	-7.514	-5.965	-7.622
6.5	5.00	0.277	-3.698	-9.837	-3.231	-6.752	-5.360	-6.755
6.5	5.50	0.226	-3.320	-8.779	-2.952	-6.104	-4.829	-6.029
6.5	6.00	0.187	-2.971	-7.888	-2.688	-5.541	-4.358	-5.410
6.5	6.50	0.157	-2.650	-7.126	-2.439	-5.045	-3.934	-4.873
6.5	7.00	0.134	-2.353	-6.464	-2.204	-4.601	-3.551	-4.400
6.5	7.50	0.115	-2.077	-5.881	-1.983	-4.199	-3.202	-3.978
6.5	8.00	0.100	-1.820	-5.363	-1.773	-3.833	-2.881	-3.598
6.5	8.50	0.088	-1.581	-4.898	-1.574	-3.496	-2.586	-3.253
6.5	9.00	0.078	-1.356	-4.477	-1.384	-3.183	-2.312	-2.937
6.5	9.50	0.069	-1.146	-4.094	-1.202	-2.892	-2.057	-2.645
6.5	10.00	0.062	-0.947	-3.743	-1.028	-2.620	-1.818	-2.375
6.5	15.00	0.027	0.556	-1.328	0.426	-0.601	-0.039	-0.430
6.5	20.00	0.015	1.530	0.081	1.481	0.675	1.094	0.776
6.5	25.00	0.010	2.235	1.051	2.263	1.569	1.896	1.628
6.5	30.00	0.007	2.784	1.785	2.866	2.242	2.509	2.281
7.0	0.50	1.217	-17.541	-99.304	-5.049	-51.753	-36.865	-62.102
7.0	1.00	1.200	-10.387	-52.135	-4.985	-29.221	-20.275	-33.771
7.0	1.50	1.173	-7.919	-35.664	-4.870	-21.054	-14.341	-23.569
7.0	2.00	1.133	-6.587	-27.040	-4.628	-16.515	-11.215	-18.157
7.0	2.50	1.083	-5.695	-21.706	-4.280	-13.657	-9.256	-14.751
7.0	3.00	1.021	-5.019	-18.043	-3.922	-11.670	-7.898	-12.381
7.0	3.50	0.950	-4.475	-15.349	-3.600	-10.177	-6.890	-10.614
7.0	4.00	0.871	-4.021	-13.272	-3.316	-8.991	-6.106	-9.230
7.0	4.50	0.785	-3.630	-11.616	-3.062	-8.010	-5.470	-8.105
7.0	5.00	0.698	-3.285	-10.262	-2.831	-7.177	-4.937	-7.169
7.0	5.50	0.613	-2.974	-9.133	-2.615	-6.458	-4.476	-6.376
7.0	6.00	0.534	-2.687	-8.180	-2.409	-5.832	-4.067	-5.696
7.0	6.50	0.465	-2.417	-7.364	-2.210	-5.283	-3.697	-5.107
7.0	7.00	0.404	-2.162	-6.659	-2.016	-4.795	-3.357	-4.591
7.0	7.50	0.353	-1.921	-6.041	-1.828	-4.359	-3.043	-4.135
7.0	8.00	0.310	-1.691	-5.495	-1.645	-3.965	-2.750	-3.728
7.0	8.50	0.274	-1.473	-5.008	-1.467	-3.606	-2.476	-3.361
7.0	9.00	0.244	-1.266	-4.570	-1.294	-3.276	-2.220	-3.028
7.0	9.50	0.218	-1.069	-4.173	-1.126	-2.971	-1.978	-2.723
7.0	10.00	0.196	-0.881	-3.810	-0.962	-2.688	-1.751	-2.442
7.0	15.00	0.085	0.575	-1.347	0.445	-0.621	-0.020	-0.449
7.0	20.00	0.047	1.538	0.073	1.489	0.666	1.102	0.768
7.0	25.00	0.030	2.239	1.047	2.267	1.564	1.900	1.624
7.0	30.00	0.021	2.786	1.783	2.868	2.239	2.511	2.279